MDPI

Article

Origins of Colour of Smithsonite from Yunnan, China

Wei Ding [1], Quanli Chen [1,*], Yan Li [1] and Xianyu Liu [2]

1. Gemmological Institute and Center for Innovative Gem Testing Technology, China University of Geosciences, Wuhan 430074, China
2. College of Jewelry, Shanghai Jianqiao University, Shanghai 201306, China
* Correspondence: chenquanli@cug.edu.cn

Abstract: Smithsonite exhibits an extensive range of colours in nature. The internal features, spectral characteristic, and trace elements of several coloured smithsonites (e.g., white, blue, blue-green, yellow, orange, and pink) from Lanping District, Yunnan Province, China, were analysed and the relationship between smithsonite colour and trace elements and/or impurities was discussed in this research. The presence of iron and manganese was closely associated with the yellow colour. Yellow greenockite grains scattered throughout parts of yellow smithsonites, ranging in size from sub-microscopic to 15 μm, efficiently changed the orange or yellow colour to "turkey fat" (a bright yellow variety of smithsonite resembling turkey fat in colour and botryoidal form) yellow. Pink colour in smithsonite was due to the presence of manganese ions. The main internal features in blue and blue-green samples were small interwoven acicular aurichalcite inclusions and alternating layers of aurichalcite–hemimorphite. Different proportions of the hole $(CO_3)^-$ radicals, copper ions (nano-sized Cu-rich inclusions), and aurichalcite inclusions created green to blue coloration variations in smithsonite. The blue–green colour change was mainly caused by aurichalcite and hemimorphite, detected with a Raman test and chemical composition test.

Keywords: coloured smithsonite; trace elements; origins; Yunnan

1. Introduction

Smithsonite is a natural anhydrous zinc carbonate ($ZnCO_3$) that is not commonly encountered in the gem trade. It belongs to the calcite group of carbonate minerals [1]. The mineral was named for James Smithson, a mineralogist and the benefactor of the Smithsonian Institution. Smithsonite as a variety of coloured gemstone has been deeply loved by people since ancient times. In the past, the best-known source of smithsonite was Greece. The Greeks called this stone Kadmeia, which means the stone of Cadmus. Thebai (Cadmus), who appeared in Greek mythology, was particularly fond of the bright, soft pinks and blues of the stones. Smithsonite is originally a colourless to white mineral, but it is very easy to integrate impurity elements into the crystal structure. When it contains a small amount of metal ions, most of it will appear coloured, including deep yellows, blues, greens, pinks, and purples. Moreover, it is renowned for its pearly lustre. However, its low hardness (4–4½ on the Mohs scale) and perfect cleavage on $\{10\bar{1}1\}$ make it often used as collector's stones (Figure 1) [2]. For many years, collectors have prized blue and blue-green smithsonites from New Mexico, USA and yellowish green factable crystals from Tsumeb, Namibia. Transparent gem-quality single-crystal smithsonites (Figure 2) are very rare and valuable. A botryoidal variety of smithsonite coloured bright yellow is known as "turkey fat." Smithsonite is also a traditional Chinese medicine with detoxification, antisepsis, and other effects, known as "calamine."

Few studies have been undertaken to explain the colours of the minerals, even though chemical analyses of the coloured smithsonites have been undertaken [3–6]. Many open questions remain as to the relationships between the colour and minor impurities of smithsonite. This article investigated Lanping smithsonite through analysing its internal

inclusion, gemmological, spectral, and compositional characteristics and explained the origins of different smithsonite colours.

Figure 1. Smithsonite mineral specimens from Yunnan, China (39.5, 36.2 and 23.8 cm high, from left to right). Specimens and photo courtesy of Y.S. Gu.
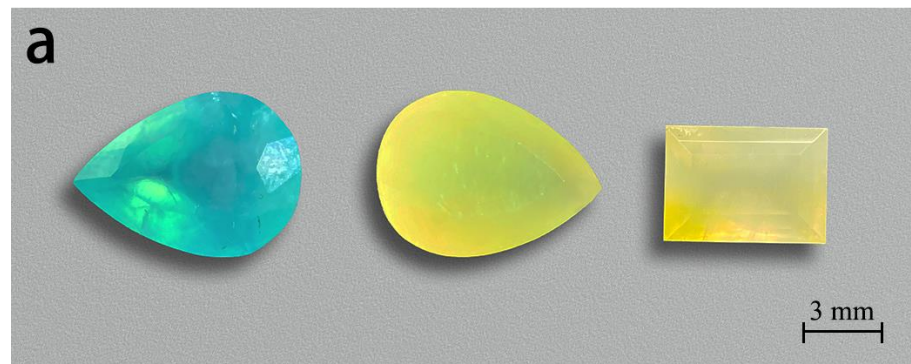

Figure 2. Smithsonites display various colours. These faceted gem smithsonites (**a**), (2.61, 1.50, 2.43 ct, from left to right) and cabochon smithsonites (**b**) range from 2.70 to 10.55 ct. All smithsonites from Lanping, Yunnan except the blue faceted smithsonite from Madagascar. Photos by Wei Ding.

2. Location and Geology

A variety of mineral resources have been discovered in deposits from Lanping, Yunnan Province, and are mostly composed of several metal ores, such as lead, zinc, silver, copper, cobalt, etc. The sulfide minerals include galena, sphalerite, pyrite, marcasite, etc., and the oxide minerals are usually distributed in the supergenic zones of the deposit, including

sulfate, carbonate, silicate of Zn and Pb, etc. Cu, Pb, and Zn are mainly distributed in the northern and southern areas of Lanping Basin. The majority of the copper and silver deposits are located in the northern part covering the Sanshan, Baiyangping, and Xiaoheqing areas. Most lead and zinc deposits are in the southern part, including the Jinding and Baiyangchang areas [7,8].

Smithsonite in Lanping Basin is mostly found in a Pb–Zn deposit in Jinding (Figure 3). The deposit is located in the centre of the northern part of the Meso-Cenozoic Lanping Basin, which belongs to the middle part of the Sanjiang Tethys orogenic belt of southwest China [9]. Moreover, the formation of the Jinding deposit was also affected by the Jinshajiang–Ailaoshan fault zone from the east and Lancangjiang fault zone from west. The ore body is found in a fractured zone between limestone strata in the upper Triassic series [10].
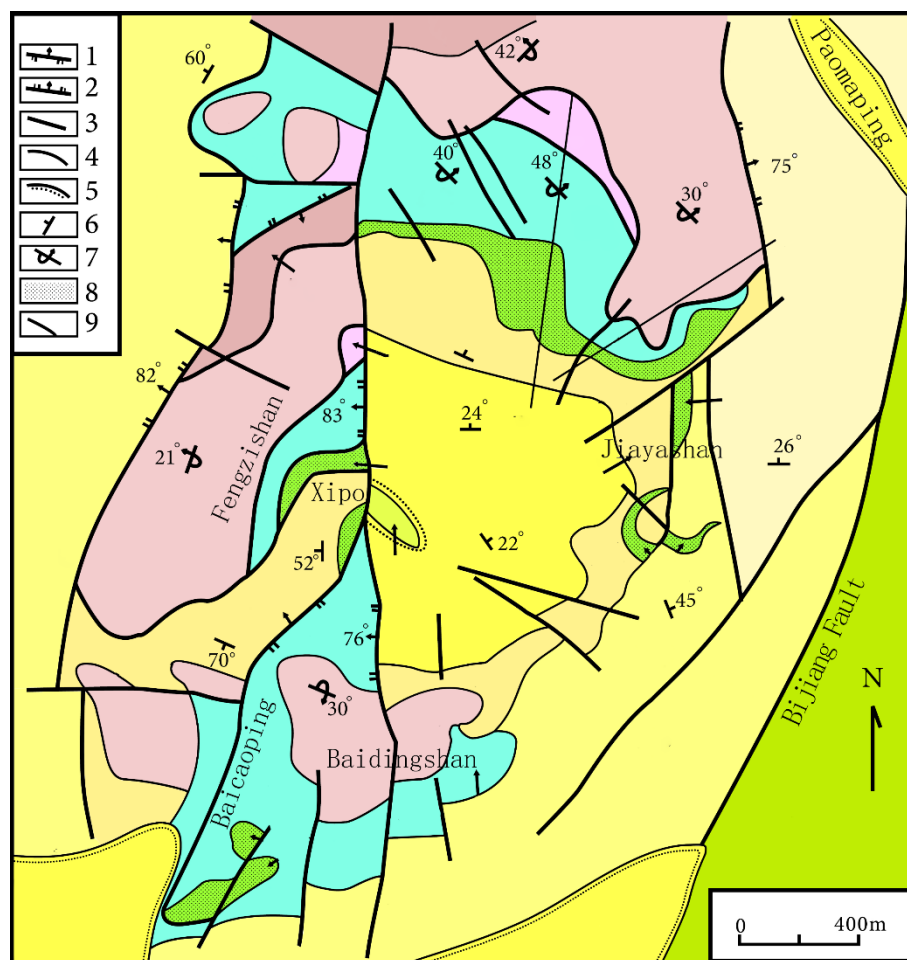

Figure 3. Geological sketch map of the Jinding Zn–Pb deposit. 1. Thrusting napped fault; 2. Normal fault; 3. Undetermined fault; 4. Geological boundary; 5. Unconformity; 6. Attitude of normal stratum; 7. Attitude of reversed stratum; 8. Lead–zinc orebody; 9. Exploration line and serial number. The geologic map of the Jinding Zn–Pb deposit was modified from [8]. Reproduced with permission from Chen, S.F.; Contribution to The Geology of The Qinghai–Xizang (Tibet) Plateau; published by Geology Press, 1991.

The Jinding deposit should be categorized as a superficial deposit that was formed through direct sulphide metasomatism. The ores can be subdivided into sandstone-type and limestone-breccia-type, based on features such as sandstone metasomatized by hydrothermal minerals (sphalerite, galena and etc.) in the vein texture or disseminated structure, and carbonate colloid in limestone breccia. Smithsonite found in this locality is generated as the zinc sulphate produced from sphalerite oxidation reacts with calcites and

other carbonates from the surrounding rock. Moreover, this process produces common paragenetic minerals such as hemimorphite and hydrozincite [11].

3. Materials and Characterization Methods

Nine rough smithsonite specimens from Lanping, Yunnan of various colours were collected for this research (Figure 4) and were classified into different varieties: blue (labelled as BL-1, 34.99 g), cyan (labelled as CY-1 and CY -2, 30.85–45.02 g), light pink to pink (labelled as PI-1 and PI-2, 6.59–11.87 g), light yellow to orange (labelled as OR-1 to OR-3, 25.06–90.89 g), and white (labelled as WH-1, 498.82 g). From these nine samples, five representative rough specimens with different colours were fabricated as optical wafers for detailed examinations.

Figure 4. Smithsonite samples from Lanping, Yunnan. Photo by Wei Ding.

Specific gravity (SG) values were determined using hydrostatic weighing. The luminescence of all samples was observed with a standard long-wave (LW, 365 nm) and short-wave (SW, 254 nm) ultraviolet (UV) lamp. Microscopic observation and photography were accomplished with a Leica M205 microscope equipped with reflected and transmitted illumination to analyse inclusions.

Infrared reflection spectra in the 500–4000 cm^{-1} range for samples with five different colours were recorded with smooth faces at 8 cm^{-1} resolution and 12 accumulations using a Vertex-80 FTIR spectrometer (BRUKER OPTICS, Billerica, MA, USA). Ultraviolet-visible (UV-Vis) absorption spectra were obtained in the range of 200–1000 nm (optimized for the 250–800 nm range) using a JASCO MSV-5200 spectrometer with a resolution of 1 nm to determine the origin of different colours in smithsonite. Raman spectra were tested in the range of 150–1500 cm^{-1} with a Horiba LabRAM HR evolution micro-Raman spectrometer with a 532 nm laser. The laser energy was 20 mV with a 10 s integration time and five scan accumulations. Spectra were compared according to the RRUFF database [12].

A JXA-8230 electron microprobe analysis (EPMA) with energy-dispersive X-ray spectroscopy (EDS) (JEOL, Tokyo, Japan) was used to obtain chemical compositions of five specimens with different colours, determine the distribution of minor and trace elements in the smithsonite's structure, and also examine other mineral inclusions. The information about internal features was also present in backscattered-electron (BSE) images. The beam voltage was 15 kV, with a 20 nA beam current and a 3 μm focused diameter.

4. Results

4.1. Gemmological Properties

All the smithsonite samples are semitransparent to subtranslucent with waxy to oily luster. The rough samples are dense clumps, botryoidal, and crustiform aggregates. Spot-RI values range from 1.61 to 1.63, hydrostatic SG values vary between 4.26 and 4.37, and the Mohs hardness is about 4 to 5. All of the samples are inert under long-wave ultraviolet (LWUV). The white samples have weak purple fluorescence under short-wave ultraviolet (SWUV), blue and green samples have blue-purple fluorescence under SWUV, and the pink and yellow samples have weak to moderate orange-red fluorescence under SWUV.

Several thin-polished sections of the specimens show clear zoning. The boundaries between the bands are distinct. The morphology, size, and arrangement of crystal particles in different bands are different. The colour textures in most samples are characterised by banded patterns with different shades of colour and variable thickness (Figures 4 and 5a,f). The morphological differences in mineral aggregates between different bands indicate that Lanping smithsonite was formed in different periods of the supergene oxidation zone. The variation in element content, temperature, and pressure in ore-forming fluid resulted in different colours of minerals [13].
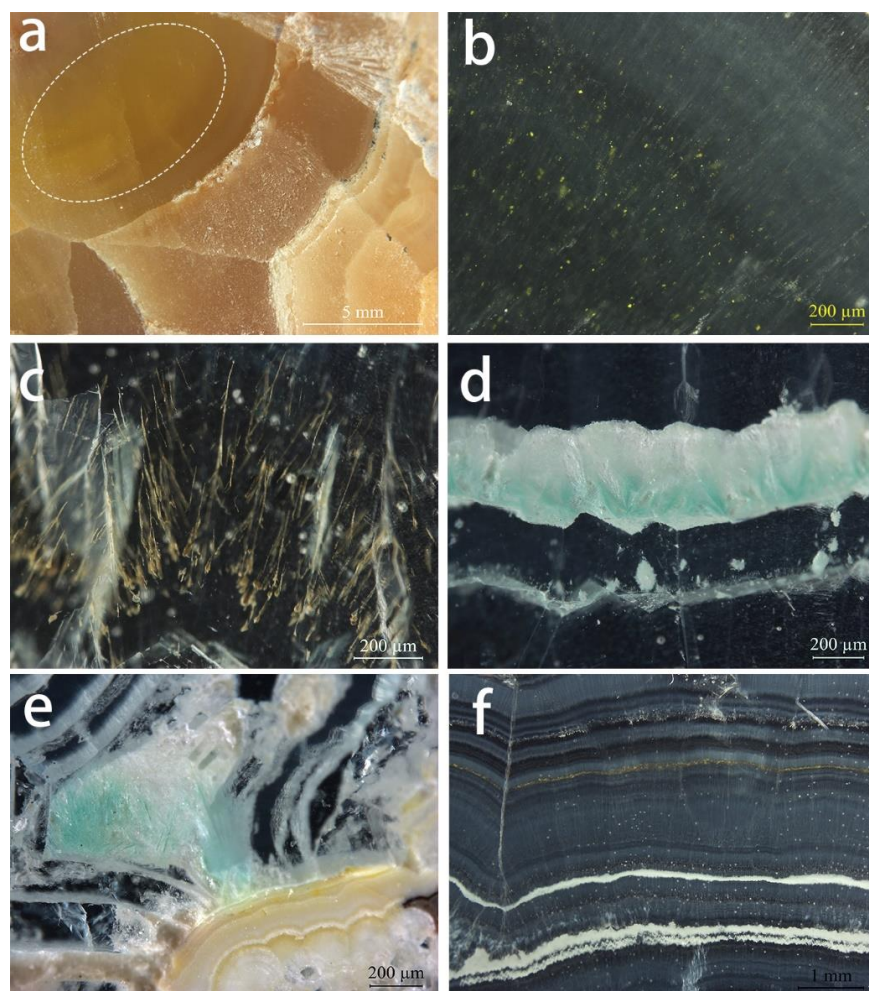

Figure 5. Internal features observed in Lanping smithsonite samples: (**a**) Yellow smithsonite section with stripes of different colour. The white oval corresponds to the location of b. (**b**) Yellow mineral grains in the dark yellow region of the yellow sample. (**c**) Dendritic yellow inclusions in cyan smithsonite. (**d**) Fibrous blue-green inclusions in cyan smithsonite. (**e**) Blue-green fibrous inclusions and light yellowish white mineral layers in the blue sample. (**f**) Alternations of smithsonite with different shades and white–yellowish-brown layers in the pink sample section. Photos by Wei Ding.

There are no fluid inclusions in these Lanping smithsonite specimens, which are dominated by solid inclusions and colour zoning. The granular yellow inclusions (Figure 5b) are dispersed in yellow smithsonites with the range of sub-microscopic to 15 μm and produce a yellower hue compared to areas without the inclusion. The cyan specimens contain randomly oriented dendritic yellow (Figure 5c) and fibrous blue inclusions along the direction of the layer structure (Figure 5d). Fibrous blue inclusions are also present in the blue samples, but in smaller quantities (Figure 5e).

4.2. Spectroscopy

The reflectance FTIR spectra show (Figure 6) the broadly strong band at about 1521 cm^{-1} associated with the asymmetric stretching vibration of CO_3^{2-}. Relatively strong bands near 871 and 743 cm^{-1} are related to the in-plane bending vibration and out-of-plane bending vibration of CO_3^{2-}, respectively [14].
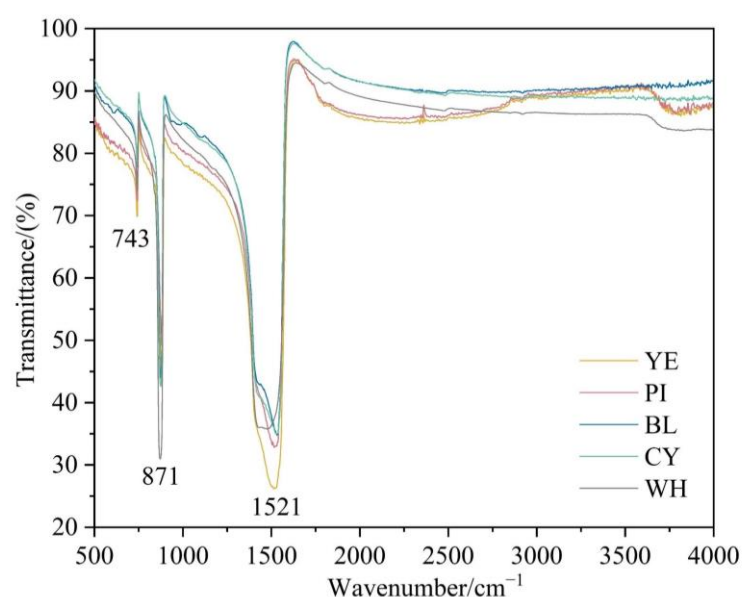

Figure 6. FTIR spectra of smithsonite samples in the range of 500–4000 cm^{-1}.

Figure 7 compares the absorption spectra of five representative colours. The test samples were too thick to obtain an optical absorption spectrum with an adequate signal-to-noise ratio; hence, some weak absorption features were too weak to be obtained. The spectrum of yellow smithsonite was recorded with a strong absorption band centred at ~446–450 nm, a steady increase in absorption from the near infrared towards the UV region, and weak bands at 281 and 448 nm. The 448 nm band was the main cause of yellow colour in smithsonite. The pink colouration is related to a broad, asymmetric band at ~300–490 nm and a slightly weak band at 590 nm. Similar features would be expected to colour pink to orangey pink in rhodochrosite, which is richer in Mn^{2+} [15]. Both blue and cyan samples showed similar absorptions in their UV-Vis–NIR spectra. The 352 nm peak of the blue sample was more or less covered by the absorption edge in the violet-blue region. In contrast, the absorption edge of the 317 nm peak of the cyan sample shifted to a longer wavelength from the violet-blue region to the blue region. The blue material showed a gradual increase in absorption from 550 to 900 nm, while the cyan sample displayed a slight gradual increase in absorption from 600 towards longer wavelengths. In the cyan sample, bands absorbed more blue and less yellow, thus leading to a yellower hue that shifts the blue colour towards cyan. In white smithsonite, there were no absorption peaks in the visible light region, which did not lead to any apparent colour.
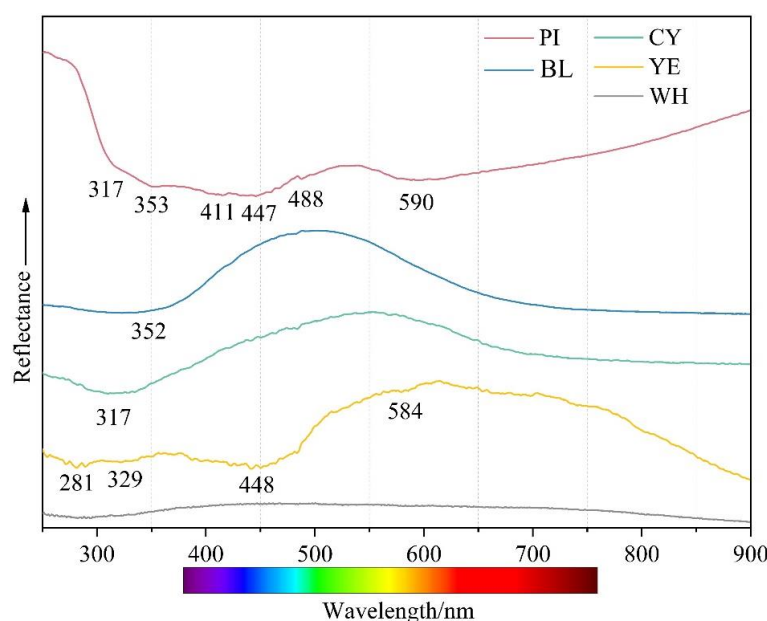
Figure 7. UV-Vis spectra of smithsonite samples with five colours.

Raman spectroscopy of smithsonite samples with different colours revealed distinct carbonate features. The positions of these bands were quite similar among samples, although differences in the spectra were exhibited by the width and intensity of some peaks. The Raman spectra showed an intense sharp band at 1093 cm^{-1} and additional peaks at 197, 305, 731, 1407, and 1737 cm^{-1} (Figure 8). The band at 1093 cm^{-1} was assigned to the v_1 symmetric stretching mode of the carbonate unit. Raman bands at 1407 and 731 cm^{-1} were ascribed to the v_3 (CO3)$^{2-}$ antisymmetric stretching modes and the carbonate v_4 in phase bending modes, respectively. Bands centred at approximately 305 and 197 cm^{-1} belong to lattice modes [16].
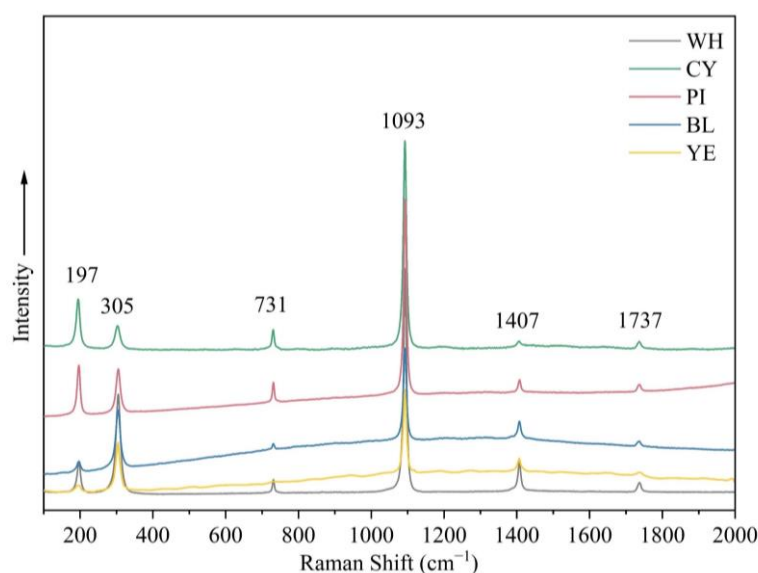

Figure 8. Raman spectra of samples in five colours in the range 100–2000 cm^{-1} show features associated with CO$_3{}^{2-}$ as well as lattice modes.

Several mineral inclusions were also found in the smithsonite with Raman spectroscopy (Figure 9). The Raman spectra of the yellow mineral inclusions matched that of greenockite (Figure 9a). The Raman shifts (Figure 9b) of the fibrous blue inclusions in the

cyan sample provided a good fit with aurichalcite. In addition, the dendritic brown inclusions in the cyan sample are speculated to be a pyrochlore-supergroup mineral according to Raman shifts (Figure 9c).
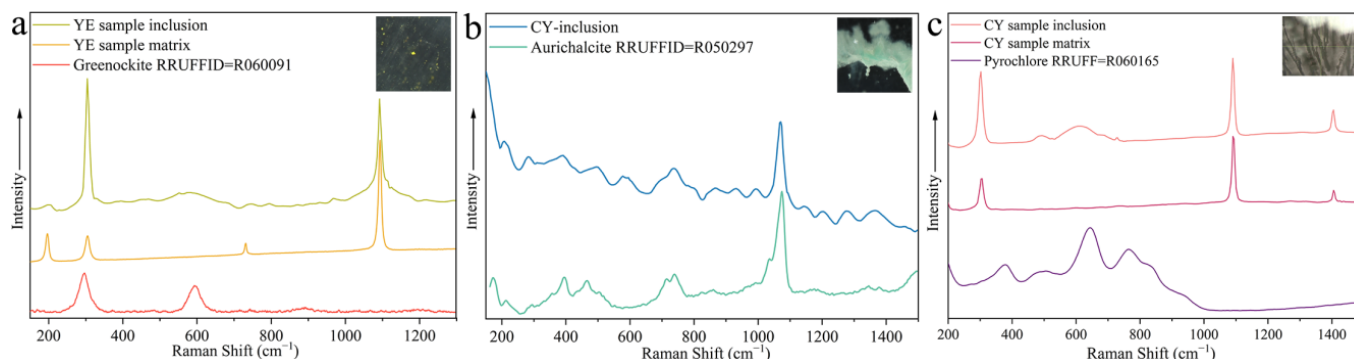

Figure 9. Raman spectra of mineral inclusions, together with spectrum of the host smithsonite. (**a**) A yellow greenockite inclusion in the yellow sample (**b**) a blue fibrous aurichalcite inclusion in the cyan sample, and (**c**) a brown dendritic pyrochlore-supergroup mineral inclusion in the cyan sample. Raman spectra of the host smithsonite, RRUFF greenockite sample R060091, aurichalcite sample R050297, and pyrochlore sample R060165 for comparison. Inset photomicrographs by Wei Ding.

4.3. Chemical Composition

The chemical compositions of these specimens are summarised in Table 1. These Lanping smithsonite specimens generally contained about 63 wt% ZnO and 35 wt% CO_2. The detected non-formula metallic elements were Ca, Cd, Pb, Mg, Fe, Mn, Cr, and Cu (Table 1), originating from either primary sulphide ores or the ore body or parent rocks leached by groundwater [10]. Ca, Cd, and Mg cations can be incorporated in $ZnCO_3$ to form various solid solutions due to the structural similarities of smithsonite, calcite, otavite, and magnesite. Ca as the main trace element in all samples ranged from 0.19 to 2.23 wt%. Most samples also presented varying concentrations of Cd (up to 1.08 wt%) and Pb (up to 1.07 wt%). Iron and manganese were commonly detected, with values of 0.01–0.52 wt% for FeO (with the total Fe expressed as FeO) and 0.06–0.19 wt% for MnO. Some samples detected Mg (<0.04 wt%) and Cr (<0.03 wt%) contents. Copper was below the detection limit in almost all the samples. Only trace amounts of CuO (1.01 and 0.63 wt%, respectively) were detected in blue and cyan smithsonites.

Table 1. Electron microprobe analyses of smithsonite samples (wt%).

Sample	WH-1	WH-2	YE3-1	YE3-2	YE1-1	PI-1	PI-2	PI-3	BL-01	CY-1
Colour	White	White	Light orange -yellow	Light orange -yellow	Yellow	Whitish pink	Pink	Dark pink	Blue	Bluish green
CaO	0.53	0.64	1.42	0.37	2.23	2.17	0.45	0.19	0.2	0.81
CdO	0.05	-	0.77	1.08	0.26	-	-	0.223	0.68	0.41
PbO	-	0.14	0.21	1.02	0.05	-	0.19	0.76	1.07	0.24
MgO	0.01	0.01	-	-	-	-	0.03	0.03	0.02	0.04
FeO	0.52	0.5	0.15	0.14	0.61	0.01	0.13	0.17	-	-
MnO	0.15	0.11	0.15	0.09	0.14	0.06	0.08	0.19	-	-
Cr_2O_3	-	-	-	-	0.03	-	-	-	-	0.02
CuO	-	-	-	-	-	-	-	-	1.01	0.63
ZnO	63.01	62.81	61.87	62.57	61.69	62.08	63.88	63.79	61.7	62.35
CO_2	34.94	34.88	35.07	34.85	35.71	35.32	35.11	35.13	34.55	34.6
Total	99.22	99.09	99.65	100.13	100.72	99.64	99.88	100.48	99.23	99.08
Visible inclusions	-	-	-	-	Greenockite	-	-	-	Aurichalcite	Aurichalcite

Generally, the high variation in trace elements within and among samples and the BSE images of the samples indicate that the Lanping smithsonite has a relatively heterogeneous

chemical composition. The presence of lead, iron, and calcium is related to the high local ore content. The occurrence and content of trace elements reflect the differences between fluid activities and trace elements carried by fluids [13].

The compositions of the different mineral inclusions in the smithsonites were confirmed using EPMA-EDS. The inclusions were available for visualization and identification with BSE imaging (Figure 10). The aggregates of the mineral inclusions consisted of greenockite, aurichalcite, hemimorphite, and otavite.
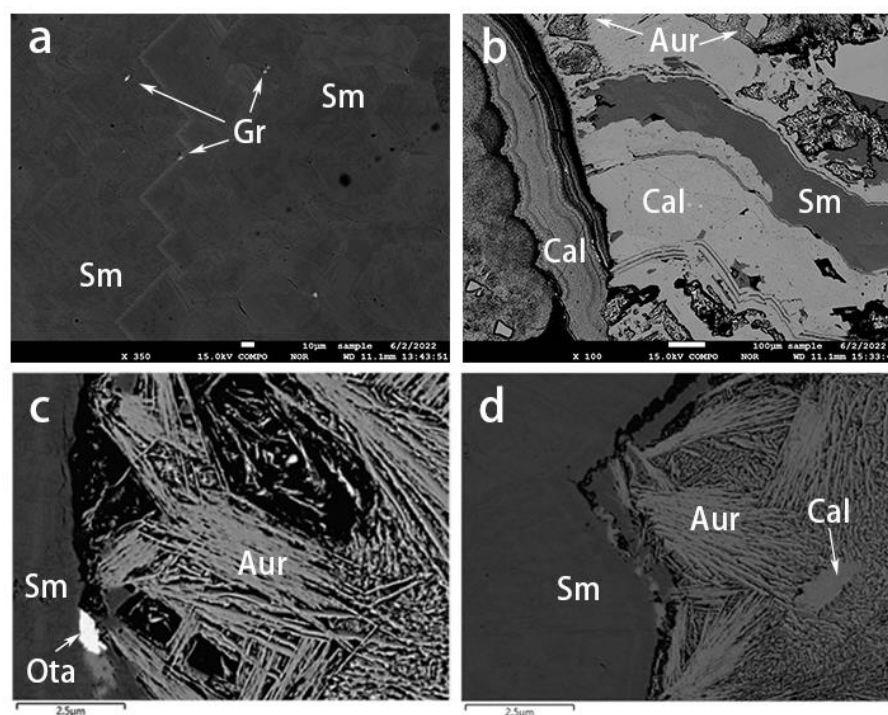

Figure 10. BSE images of smithsonite samples. (**a**) Greenockite grains within yellow smithsonite. (**b**) Alternations of blue smithsonite and aurichalcite–hemimorphite layers. (**c**) An otavite inclusion and (**d**) development of aurichalcite–hemimorphite layers in the cyan smithsonite. Sm: smithsonite, Gr: greenockite, Aur: aurichalcite, Cal: hemimorphite, Ota: otavite.

Greenockite (CdS) was only detected in the yellow sample (Figure 10a) and also comprised the granular yellow aggregates described above (Figure 5a). Aurichalcite ((Zn, Cu^{2+})$_5$(CO_3)$_2$(OH)$_6$) was found as blue or green crusts or mats of tiny acicular crystals (Figures 5d,e and 10c,d) developed between the blue and green-blue smithsonite layers. The hemimorphite ($Zn_4Si_2O_7$(OH)$_2$) either existed in the aurichalcite layer (Figure 10b) or developed as alternating layers with smithsonite (Figure 10d). We also observed the presence of otavite ($CdCO_3$, Figure 10c) as an epitaxial mineral.

5. Discussion

Common carbonate minerals are calcite, magnesite, rhodochrosite, smithsonite, and siderite. Calcite mined from uranium ore deposits or irradiated artificially can be coloured due to a radiation-induced colour centre. The CO_3^{3-} electron centre is related to the ionization of lead ions and the electrons tapped by CO_3^{3-} The centre absorbs energy in the green region of the spectrum, giving calcite a rose red colour. The purple colour of calcite is caused by a CO_3^{3-} electron centre and O^- hole centre associated with rare earth impurity elements, while the yellow colour is primarily caused by a CO_3^- hole centre [17]. Rhodochrosite is mostly pink to orange due to the electronic transition of Mn^{2+} [15,18].

Pure smithsonite with the chemical formula $ZnCO_3$ is entirely colourless. Minor impurities, such as trace elements, point defects, and inclusions, cause colours in smith-

sonite. Lanping smithsonite samples with different colours had some obvious differences in inclusions (Figure 5), UV-Vis spectra (Figure 7), and chemical composition (see Table 1).

The iron concentration and smithsonite's yellow colour showed an approximately positive relationship. The absorption peaks in the ultraviolet and blue regions are related to the trapped hole paired with Fe^{3+} [19]. Manganese is also a vital colouring element in smithsonite. Moreover, there is no obvious correlation between the manganese content and coloration in the investigated yellow samples (Table 1 and Figure 5). The absorption peaks at 448 and 584 nm in the UV-Vis spectrum are attributed to Mn^{2+} [15] and result in the absorption of mainly blue and a few orange-red wavelengths. The electron paramagnetic resonance (EPR) test results showed that the dark yellow-green coloration of smithsonite from the same origin is the result of the d-d electronic transition of Fe^{3+} and Mn^{2+} [3]. The average content of iron and manganese (FeO 0.95%, MnO 0.46%) is significantly higher than that of the yellow variety in this paper. The identical multiple chromophores present in different colours of smithsonite may be due to the different contents and proportions of impurity elements. Cadmium has been reported to be one of the causes of the yellow colour of smithsonite [4]. In this paper, EPMA results showed that most samples contained cadmium, and cadmium content was not directly related to the colour. Yellow smithsonite loses its orange tint and produces the "turkey oil" yellow colour, which is only related to the presence of greenockite (CdS) inclusions. It should be mentioned here that the content of iron and manganese in the white sample is close to that in the yellow sample, but the white colour contradicts the conclusion that iron and manganese produce yellow colour, presumably because iron and manganese ions have different valence states in the white and yellow varieties.

It was often assumed that manganese was primarily responsible for pink to red in some carbonate minerals, such as rhodochrosite [18]. This difference in manganese was evident in the colouration of the pink variety and the regular increase in MnO from the light colour zone (point PI-1 0.06 wt%) to point PI-3 (0.19 wt%). The absorption peaks of the pink variety in the UV-Vis spectrum (Figure 7) is consistent with a series of Mn^{2+}-related absorptions. The absorbing addition in the blue and red regions of the spectrum creates magenta, consistent with the pink colour of some rhodochrosite. The absorption features indicated that manganese ions in pink smithsonite play a role in the coloration, and the valence or occupancy of Mn^{2+} ions may be similar to that in rhodochrosite. Another possible cause of the pink colour of smithsonite is the elevated presence of lead. Lead may act as a chromophore element to give some carbonate minerals a pink to purple colour [17]. The lead content was also positively correlated with the shade of colour, although the EPMA test failed to detect the presence of lead in the lighter pink area.

Among the transition metal ions, copper can generally substitute the principal elements and change the minerals colour to blue-green. Lanping blue smithsonite showed substantially higher copper concentrations compared with other colour samples. Because of the absence of anhydrous divalent copper carbonates, the blue colour of smithsonite is caused by the nano-sized (3–7 nm, mainly Si/Ca/Cu/As-rich) Cu-rich inclusions rather than substitution of zinc cations by copper cations [5]. In the blue variety, visible aurichalcite inclusions were detected, affecting the colour. Another nature of blue colour in smithsonite was related to point defects. The presence of $(CO_3)^-$ radical anions causes many carbonate-containing minerals to produce blue and green (as a mixture of blue and yellow), such as blue irradiated calcite and cancrinite [20]. The Raman spectra of blue and green smithsonite samples (Figure 8) showed very weak bands at about 1200 cm^{-1} that can correspond to $(CO_3)^-$ [21]. Therefore, the blue color of smithsonite is caused by a combination of the hole $(CO_3)^-$ radicals, numerous nano-sized Cu-rich inclusions, and aurichalcite inclusion in the crystals.

The blue-green cooler in smithsonite is due to the presence of $(CO_3)^-$ radicals, the relatively low copper amount, and inclusions or alternating layers of aurichalcite (Figrues 5d,e and 10c,d) formed by precipitation and sedimentation of different fluids. The $(CO_3)^-$ radicals and copper probably have a minor influence on the greenish coloration

of the investigated smithsonite because the cyan colour of smithsonite is closer to the inclusion colour.

In addition to the inclusions mentioned above, colour can also be caused by other impurities. For example, smithsonites from Lavrion, Greece, changed colour to dark green because of galena grains. Moreover, the presence of Mn–Fe–Pb oxides and hydroxides creates orange and brown colours [6].

6. Conclusions

In general, chromophore mineral impurities and zinc substitution by metallic cations are the two main causes of colouration in the beautiful Lanping smithsonites. Point defects also play a role in the colour change. In order to understand the chromophores and colour characteristics, the internal features, quantitative chemistry, and spectral properties of colourful smithsonite were discussed in this research. These smithsonite varieties contain more than one colour-causing agent. Moreover, trace elements can be the direct cause of colour. Iron and manganese are enriched in orange-yellow smithsonites. The Cd^{2+} ion itself is not the cause of colour; only the presence of greenockite inclusions is related to "turkey fat" yellow in smithsonite. Manganese substitution of zinc is limited and changes the colour of smithsonite to pink.

Only blue and cyan (blue-green) smithsonite samples contain weak Raman peaks at around 1200 cm^{-1} and Cu^{2+} concentrations higher than the detection limit of the test. The blue and cyan (blue-green) colours are both due to the $(CO_3)^-$ radicals, nano-sized inclusions formed by Cu^{2+} ions, and aurichalcite inclusions (or aurichalcite–hemimorphite layers). As for the cyan smithsonite, the aurichalcite–hemimorphite layers are the major factor affecting colour.

Author Contributions: Conceptualization, Q.C. and X.L.; methodology, Q.C.; software, W.D.; validation, Q.C., W.D. and X.L.; formal analysis, W.D.; investigation, Q.C.; resources, X.L.; data curation, X.L.; writing—original draft preparation, W.D.; writing—review and editing, Y.L.; visualization, Q.C.; supervision, Y.L.; project administration, Q.C. and X.L.; funding acquisition, Q.C. All authors have read and agreed to the published version of the manuscript.

References

1. Reeder, R.J. Crystal chemistry of the rhombohedral carbonates. *Rev. Mineral. Geochem.* **1983**, *11*, 1–47.
2. Anthony, J.W.; Bideaux, R.A.; Bladh, K.W.; Nichols, M.C. *Handbook of Mineralogy. V. Borates, Carbonates, Sulfates*; Mineralogical Society of America: Chantilly, VA, USA, 2003; p. 223.
3. Luo, J.; Yue, S.W.; Guo, H.Y.; Liu, J.J. Spectroscopic Characteristics and Coloring Mechanism of Smithsonite Jade. *Spectrosc. Spect. Anal.* **2022**, *42*, 1886–1890.
4. Liao, B.L.; Lu, Y.J.; Li, D.S.; Zeng, W.L.; Sun, Y.; Li, X.J. The mineralogical characteristics and prospect analysis of yellow-zinc ore. *World Nonferrous Metals* **2017**, *21*, 232–234.
5. Samouhos, M.; Zavasnik, J.; Recnik, A.; Godelitsas, A.; Chatzitheodoridis, E.; Sanakis, Y. Spectroscopic and nanoscale characterization of blue-coloured smithsonite (ZnCO₃) from Lavrion historical mines (Greece). *Period. Miner.* **2015**, *84*, 373–388.
6. Katerinopoulos, A.; Christos, S.; Voudouris, P. Lavrion smithsonites: A mineralogical and mineral chemical study of their coloration. In *Mineral Deposit Research: Meeting the Global Challenge*; Springer: Berlin/Heidelberg, Germany, 2005; pp. 983–986.
7. Ye, L.; Cheng, Z.T.; Pan, Z.P.; Liu, T.G.; Gao, W. A study on the distribution characteristics and existing states of cadmium in the Jinding Pb-Zn deposit, Yunnan Province, China. *Chin. J. Geochem.* **2010**, *29*, 319–325. [CrossRef]
8. Chen, S.F. geology and metal source of Jinding strarabound Pb-Zn deposit, Lanping, Yunan. *Contrib. Geol. Qinghai-Xizang Tibet. Plateau* **1991**, *21*, 1–17.

9. Li, G.W.; Liao, Z.W. Geological Characteristics and Prospecting Direction of Lanping Copper-lead-zinc Deposit in Yunnan. *Conserv. Util. Miner. Resour.* **2012**, *5*, 13–15.

10. Xue, C.J.; Chen, Y.C.; Yang, J.M.; Wang, D.H. Analysis of ore-forming background and tectonic system of Lanping basin, Western Yunnan Province. *Miner. Depos.* **2002**, *21*, 36–44.

11. Fan, Y.B.; Li, H.; Xu, X.W.; Dong, L.H. Research status and progress of nonsulfide zinc-lead deposit. *Northwestern Geol.* **2018**, *51*, 147–159.

12. Lafuente, B.; Downs, R.T.; Yang, H.; Stone, N. The power of databases: The RRUFF project. In *Mineralogical Crystallography*; Armbruster, T., Danisi, R.M., Eds.; W. De Gruyter: Berlin, Germany, 2015; pp. 1–30.

13. Qi, Y.; Hu, R.; Gao, J.; Leng, C.; Gao, W.; Gong, H. Trace and minor elements in sulfides from the Lengshuikeng Ag–Pb–Zn deposit, South China: A LA–ICP–MS study. *Ore Geol. Rev.* **2022**, *141*, 104663. [CrossRef]

14. Frost, R.L.; Martens, W.N.; Wain, D.L.; Hales, M.C. Infrared and infrared emission spectroscopy of the zinc carbonate mineral smithsonite. *Spectrochim. Acta Part A Mol. Biomol. Spectrosc.* **2008**, *70*, 1120–1126. [CrossRef] [PubMed]

15. Zwaan, J.; Mertz-Kraus, R.; Renfro, N.D.; Mcclure, S.F.; Laurs, B.M. Rhodochrosite Gems: Properties and Provenance. *J. Gemmol.* **2018**, *36*, 332–345. [CrossRef]

16. Hales, M.C.; Frost, R.L. Synthesis and vibrational spectroscopic characterisation of synthetic hydrozincite and smithsonite. *Polyhedron* **2007**, *26*, 4955–4962. [CrossRef]

17. Zhong, M.M. Radiative coloration of calcite and apatite. *World Nucl. Geosci.* **1990**, *000*, 11–14.

18. Klein, C.; Dutrow, B. *Manual of Mineral Science*, 23rd ed.; John Wiley: New York, NY, USA, 2007; pp. 234–239.

19. Li, H.; Zu, W.D.; Yu, J.; Tang, X.L. Study and calculation of UV-Vis spectral characteristics of iron-bearing gemstones. *Guangxi J. Light Ind.* **2009**, *25*, 12–13.

20. Shendrik, R.; Kaneva, E.; Radomskaya, T.; Sharygin, I.; Marfin, A. Relationships between the structural, vibrational, and optical properties of microporous cancrinite. *Crystals* **2021**, *11*, 280. [CrossRef]

21. Kaneva, E.; Shendrik, R. Radiation defects and intrinsic luminescence of cancrinite. *J. Lumin.* **2022**, *243*, 118628. [CrossRef]